

## Thomson scattering measurements of heat flow in a laser-produced plasma

J Hawreliak<sup>1</sup>, D M Chambers<sup>2,8</sup>, S H Glenzer<sup>3</sup>, A Gouveia<sup>1</sup>,  
R J Kingham<sup>4</sup>, R S Marjoribanks<sup>5</sup>, P A Pinto<sup>2</sup>, O Renner<sup>6</sup>,  
P Soundhauss<sup>1</sup>, S Topping<sup>7</sup>, E Wolfrum<sup>1,9</sup>, P E Young<sup>3</sup> and J S Wark<sup>1</sup>

<sup>1</sup> Department of Physics, Clarendon Laboratory, University of Oxford, Parks Road, Oxford, OX1 3PU, UK

<sup>2</sup> Steward Observatory, University of Arizona, Tucson, AZ 85721, USA

<sup>3</sup> Lawrence Livermore National Laboratory, Livermore, CA 94550, USA

<sup>4</sup> Plasma Physics Group, Blackett Laboratory, Imperial College, London SW7 2BZ, UK

<sup>5</sup> Department of Physics, McLennan Physical Laboratories, University of Toronto, Toronto, Ontario, M5S 1A7, Canada

<sup>6</sup> Institute of Physics, Czech Academy of Sciences, 18221 Prague, Czech Republic

<sup>7</sup> School of Mathematics and Physics, Queens University Belfast, Belfast, BT7 1NN, UK

Received 29 January 2004

Published 23 March 2004

Online at [stacks.iop.org/JPhysB/37/1541](http://stacks.iop.org/JPhysB/37/1541) (DOI: 10.1088/0953-4075/37/7/013)

### Abstract

Measurements of the electron distribution and heat flow between the critical and ablation surfaces in a laser-produced plasma have been obtained using Thomson scattering. A frequency-quadrupled probe beam was used to obtain Thomson spectra at above-critical densities in a plasma produced by irradiation of solid targets with the fundamental laser light at irradiances of  $3 \times 10^{14} \text{ W cm}^{-2}$ . Comparison of Thomson spectra at the ion acoustic frequency (sensitive to the cold return current) with simulated spectra shows that the data are consistent with Fokker–Planck simulations of the electron distribution function, providing the first direct information on the electron distribution function.

### 1. Introduction

Thermal transport in laser-produced plasmas (LPPs) is perhaps the most important mechanism in determining the hydrodynamic properties of the laser-irradiated target [1, 2]. Plasmas generated with nanosecond laser pulses with irradiances on target between  $\sim 10^{12}$  and  $10^{15} \text{ W cm}^{-2}$  have been studied for more than three decades owing to their relevance to fields such as laser processing, inertial confinement fusion and x-ray lasers. At the lower end of this range in irradiances, the laser energy is absorbed principally by inverse bremsstrahlung, and (neglecting the effects of refraction) such absorption occurs until the

<sup>8</sup> Present address: Department of Physics, University of York, Heslington, York, YO10 5DD, UK.

<sup>9</sup> Present address: Institut für Plasmaphysik, Max-Planck-Gesellschaft, D-85748, Garching, Munich, Germany.

position in the plasma where the laser frequency equals the plasma frequency—the so-called critical density. From this point the thermal energy flows down the temperature gradient to the ablation surface. As the irradiance is increased radiation can also be absorbed by resonance absorption, depositing energy at and around the critical surface into electrons with velocities far greater than the thermal velocity. As resonance absorption deposits energy close to the critical surface, energy due to it can flow both towards and away from the target surface.

Early on in the history of this area of study, it was realized that the temperature gradient between the critical and ablation surfaces was so steep that the mean free path of the electrons could exceed the temperature gradient scale length, resulting in a breakdown of Fourier's law of conduction [3]. Indeed, a naive application of the Spitzer–Härm (SH) theory of the thermal conductivity of the plasma often predicted heat flows in excess of that equivalent to all the electrons flowing at the thermal velocity—the 'free-streaming limit' (FSL). In order to obtain agreement with experimentally measured ablation pressures and mass ablation rates, initial hydrocode modelling of the laser-plasma interaction included an *ad hoc* limit on the allowed heat flow expressed as a fraction of the FSL [4, 5]. Values placed on this flux limit ranged from approximately 0.03 to 0.15, and for some years a vigorous debate on the appropriate value ensued.

Significant progress in our understanding of heat flow in LPPs followed the development of Fokker–Planck (FP) codes which calculated the full electron distribution function [6]. These FP calculations took into account the non-local nature of the problem, and confirmed that no single flux limiter was appropriate to all experimental situations. Further developments led to the capability to include approximate models of non-local heat flow into hydrocode simulations [7–9], resulting in good agreement between predicted and experimentally measured ablation rates and pressures—the parameters that dictate the gross hydrodynamic response of the target.

However, it should be stressed that while there is currently good agreement between hydrocodes incorporating some non-local model of the heat flow (or the appropriately chosen flux limit) and experimental measurements [10, 11] of ablation pressures and mass ablation rates, no direct experimental information on the actual form of the electron distribution function between the critical and ablation surface for directly driven targets has yet been reported. Given the importance of heat flow to the whole physics of LPPs, such a deficiency is clearly undesirable.

In this paper, we present results of the first direct measurement of heat flow in a directly driven LPP using time-resolved Thomson scattering (TS) [12, 13]. The measurements are unique in two important respects. Since the TS measurements are made with a frequency-quadrupled laser beam, information on the hydrodynamics of the plasma can be obtained at and above the critical density. As there are no sources or sinks of energy in this region, once steady-state flow has been approached, the outward enthalpy flux deduced from the TS measurements can be equated with the inward heat flow. Secondly, from the TS spectra we obtain direct information on the form of the electron distribution function for electrons with velocities close to the ion acoustic wave phase velocity. The amplitude of such waves travelling towards and away from the target surface differs owing to the effect of the large cold electron return current necessary for maintaining charge neutrality as the hot electrons carry the thermal current. Subject to the caveat that the level of resonance absorption can be ignored (which we discuss in more detail below), we show that the degree of the asymmetry of the TS spectrum around these ion acoustic features, coupled with the measured heat flow, is fully consistent with an FP model, but cannot be reconciled with an SH approach. The data thus provide the first direct evidence of the validity of the FP calculations of the electron distribution function itself.

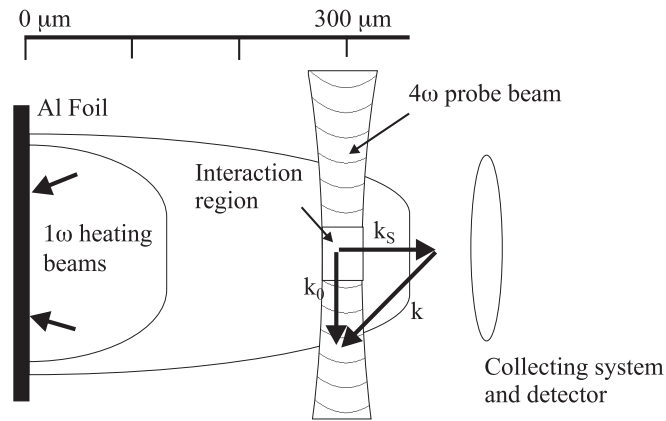


**Figure 1.** A schematic diagram of the experimental set-up.  $k_0$  is the probe wave vector,  $k_s$  is the collecting vector and  $k$  is the scattering vector.

## 2. Experiment

The experiment was performed using the VULCAN laser at the Rutherford Appleton Laboratory, UK. The experimental set-up, shown in figure 1, is designed to create a plasma which expands in a planar geometry over the region of interest. A cluster of six  $1.053\ \mu\text{m}$  laser beams were focused with  $f/10$  lenses via random phase plates to a  $500\ \mu\text{m}$  diameter spot onto  $12\ \mu\text{m}$  thick aluminium foil targets. The six beams were arranged symmetrically around the target normal, forming a cone with semi-angle of  $20^\circ$ . The total laser energy on target was  $600\ \text{J} \pm 10\%$  in a trapezoidal pulse of duration  $900\ \text{ps}$  with rise and fall times of  $100\ \text{ps}$ , producing an irradiance on target of  $3 \times 10^{14}\ \text{W cm}^{-2}$ . Another beam of  $2\ \text{ns}$  duration was frequency quadrupled to  $263.3\ \text{nm}$  ( $4\omega$ ). This beam, containing  $\sim 5\ \text{J}$  of  $4\omega$  light, was focused along a path perpendicular to the surface normal of the aluminium target with an  $f/10$  lens to a  $30\ \mu\text{m}$  focal spot size. The focus of this probe beam could be placed at a variable distance from the initial aluminium target surface. The Thomson radiation from the  $4\omega$  probe scattered along the target surface normal was collected with an  $f/10$  lens. The TS signal was image-relayed at 1:1 magnification onto the slit of a  $1\ \text{m}$  spectrometer, dispersed with a  $3600\ \text{lines mm}^{-1}$  grating and recorded on a Imacon 500 streak camera coupled to an optical CCD. The temporal resolution, set by the streak camera slit width, was approximately  $10\ \text{ps}$ . The spectral range recorded on the streak camera was from  $261.1$  to  $265.0\ \text{nm}$ . The intersection of the focal regions of the probe beam and the image on the streak camera slit width defined the volume of the plasma from which the TS signal was recorded, which is well approximated by a cylinder with the same diameter as that of the probe beam ( $30\ \mu\text{m}$ ) and length equal to the width of the streak camera slit ( $50\ \mu\text{m}$ ). Given the incident and scattered directions of the probe, the TS signal provides information on the electron distribution function projected onto the line making an angle of  $45^\circ$  to the surface normal.

## 3. Results

Figure 2 is an experimental image of the time-resolved TS spectrum from a region  $300\ \mu\text{m}$  in front of the target surface. As we will show below, we determine this to be the steady-state position of the critical density surface (where the electron density,  $n_e$ , is  $10^{21}\ \text{cm}^{-3}$ ) for the

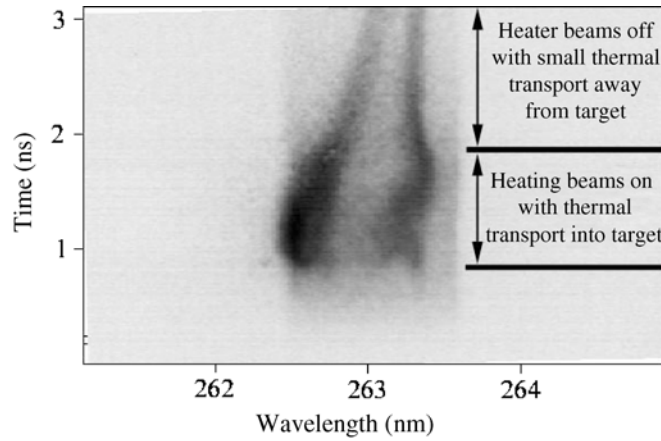


**Figure 2.** A streak record of the scattered spectrum at  $300\ \mu\text{m}$  in front of the target surface showing the ion feature.

major portion of the time while the heater beams are irradiating the target. As the heater beams form a cone with semi-angle of  $20^\circ$ , the effects of refraction within the plasma dictate that the laser light can only reach  $\sim 0.9$  of critical, and thus the heat flows through the critical density surface.

The two spectral peaks observed in the streak camera image correspond to enhanced TS due to the electrons dressing the ion acoustic waves which travel parallel and anti-parallel to the line that makes an angle of  $45^\circ$  to the surface normal. In the reference frame of the plasma, the shift in frequency from the central probe frequency,  $\omega_{ia}$ , of these ion acoustic fluctuations is given by

$$\frac{\omega_{ia}^2}{k^2} = \frac{T_e}{M_i} \left( \frac{\bar{Z}}{1 + k^2 \lambda_D^2} + \Gamma_i \frac{T_i}{T_e} \right), \quad (1)$$

where  $k$  is the magnitude of the scattering wave vector,  $T_e$  and  $T_i$  are the electron and ion temperatures, respectively,  $\lambda_D$  is the Debye length,  $M_i$  is the ion mass,  $\bar{Z}$  is the average ionic charge and  $\Gamma_i$  is the ion specific heat ratio. With the knowledge that  $\bar{Z} = 13$  (within a few per cent) from x-ray spectroscopy [14], we see that  $\omega_{ia}$  is a strong function of  $T_e$  (and only weakly dependent on  $T_i$  and  $\Gamma_i$ ). Thus, the separation of the peaks allows the determination of  $T_e$  with an accuracy which we estimate to be of order  $\pm 10\%$ . It can be seen that the central frequency between the two ion acoustic peaks is shifted from the frequency of the probe due to the Doppler shift associated with the bulk plasma motion away from the target; this provides an accurate measure of the local plasma velocity with an error of order  $\pm 4\%$ .

From figure 2 we see that while the heater beams are on, the conditions within the plasma remain approximately steady—although steady-state conditions cannot be achieved in a 1D planar plasma, at distances large compared with the focal spot size ( $\approx 1\ \text{mm}$ ) the plasma tends towards spherical expansion, and this behaviour leads to quasi steady-state behaviour within the plasma as a whole. X-ray pinhole images [15] of an aluminium dot target on a CH foil under identical experimental conditions show that at  $300\ \mu\text{m}$  the plasma expansion is 1D. As there are no sources or sinks of energy in the probed region, during this steady-state regime we can equate the outward enthalpy flux with the inward heat flow [18]:

$$Q = \rho v \left[ \frac{5}{2} \left( \frac{\bar{Z} + 1}{Am_p} \right) k_B T_e + \frac{1}{2} v^2 \right], \quad (2)$$

where  $v$  is the plasma velocity,  $\rho$  is the mass density,  $A$  is the atomic number of the ion species and  $m_p$  is the mass of a proton. The heat flow is evaluated by taking  $T_e$  and  $v$  from the TS measurements, and  $\bar{Z}$  from spatially-resolved x-ray spectroscopy [14]. In associating a single temperature,  $T_e$ , with the electrons, we are neglecting the heat flow due to the hot electrons produced by resonance absorption—a matter to which we will return in the discussion section.

The velocity can be measured from the Doppler shift of the midpoint of the Thomson scattered signal. Given the velocity at a particular point in the plasma, the density can be inferred from the knowledge of the mass ablation rate,  $\rho v$ , under these irradiance conditions. Ideally one would wish to obtain a density measurement from the electron feature in the Thomson scattering spectrum. Although this is feasible at densities well below critical (for example, under our conditions the electron feature is predicted to have a scattered intensity of 1% of the ion feature at 10% of the critical density), this feature is extremely weak above critical density. At the critical density itself, we calculate that the electron feature for the experimental conditions will be  $10^{-20}$  times the intensity of the ion feature, making it impossible to measure. Alternatively, in principle, it is also possible to estimate the electron density from an accurate knowledge of the scattered signal intensity and the scattering volume, provided one has an accurately absolutely-calibrated time-resolved detection system. As our detector and set-up were not calibrated in this way, initial estimates of the electron density based on such a method [20]<sup>10</sup> provide only order-of-magnitude estimates.

However, four independent sources of information about the densities at various points in the plasma are consistent with MEDUSA hydrocode simulations of a density profile that places the steady-state position of the critical surface  $300 \mu\text{m}$  from the target surface during the probe window. Firstly, Thomson data taken at  $z = 300 \mu\text{m}$  show the asymmetric ion feature, consistent with heat flowing down a steep temperature gradient towards the target surface. Data taken further from the target surface show no such asymmetry, consistent with the more isothermal conditions expected at below-critical densities in the coronal plasma. Secondly, the previously measured mass ablation rate for these irradiances ( $1.8 \times 10^2 \text{ kg cm}^{-2} \text{ s}^{-1}$ ) [19], with a known accuracy of  $\pm 17\%$  including uncertainties in the beam energy, combined with the measured velocities from the TS implies that the electron density  $300 \mu\text{m}$  from the surface is  $1.0(\pm 0.2) \times 10^{21} \text{ cm}^{-3}$ , i.e. the critical density. Density measurements obtained using the same method at positions closer to the target surface are also consistent with the predicted profile, but have larger error bars associated with them owing to the effects of refraction on the probe beam. Thirdly, independent electron density measurements based on the Stark broadened widths of hydrogenic [14, 16] emission lines, taken at positions between 20 and  $100 \mu\text{m}$  from the target surface are also consistent with the MEDUSA-simulated density profile. Finally, time-resolved shadowgraph images [17] taken further from the target surface, are also consistent with the same density profile. Figure 3 shows all the density data on a single graph, indicating how it is consistent with a  $1\omega$  critical density at  $300 \mu\text{m}$  from the target surface. The measured electron temperature as a function of distance from the target surface is shown in figure 4, from which we deduce that at the critical surface the temperature gradient is of order  $7 \text{ eV } \mu\text{m}^{-1}$ .

For the condition 500 ps after the heater beams are turned on, we determine a heat flux of  $6.5 \times 10^{13} \text{ W cm}^{-2} \pm 22\%$  corresponding to  $\bar{Q} = Q / (n_e m_e v_e^3) = 0.1$ , where  $n_e m_e v_e^3$  is the FSL. This heat flux is consistent with previous measurements of heat flow under similar conditions: at these irradiances  $\sim 40\%$  of the laser energy is absorbed [19], and approximately

<sup>10</sup> Estimates of the electron density from the total integrated intensity of the Thomson scattered signal in this article are only correct to an order of magnitude—the spectrometer, streak camera and CCD camera were not absolutely calibrated.

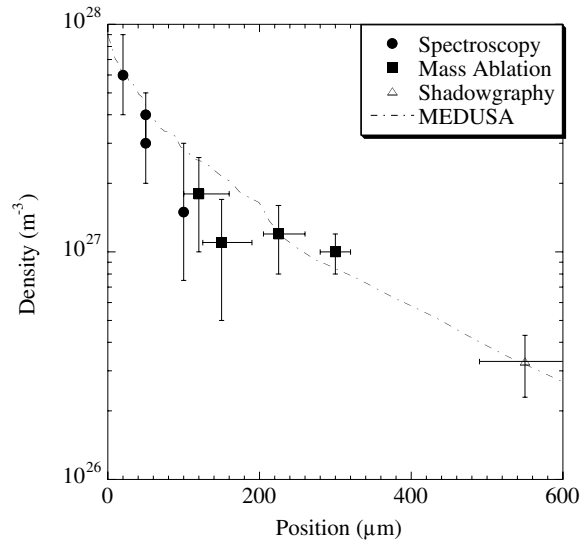


**Figure 3.** Three different measurements of the density, spectroscopy (●), mass ablation (■) and shadowgraphy (△) are shown to be consistent with a single MEDUSA density profile (— · —).

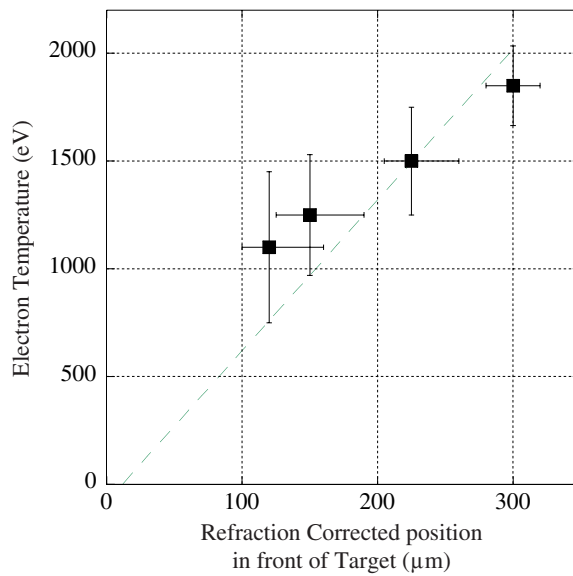


**Figure 4.** The experimental measured temperatures at different positions in front of the target surface with a dotted line showing the  $7 \text{ eV } \mu\text{m}^{-1}$  gradient.

half of this flows down towards the ablation surface, while the rest is lost in the thermal and kinetic energies of the coronal region below the critical density [18].

TS scattering not only provides data on the hydrodynamics of the plasma, but also yields information on the velocity gradient of the electron velocity distribution function at the ion acoustic wave phase velocity [21, 22]. The two ion-acoustic peaks that can be seen in figure 2 have different intensities. This asymmetry has its origin in the lack of symmetry of

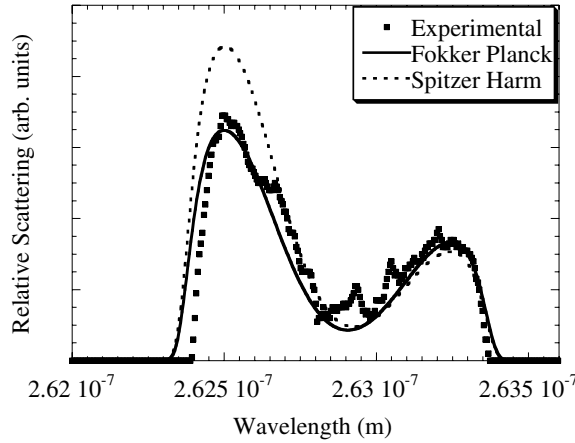


**Figure 5.** The experimental scattered spectrum along with a spectrum generated from a Fokker–Planck and Spitzer–Härm distributions for  $T_e = 1850$  eV,  $n_e = 1.0 \times 10^{21}$  cm $^{-3}$  and  $Q = 6.5 \times 10^{13}$  W cm $^{-2}$ .

the distribution function itself: at velocities corresponding to the phase velocity of the ion acoustic waves, there are more electrons that are travelling away from the target surface than towards it, as a large number of relatively cold electrons flow away from the target surface to maintain charge neutrality as the hot electrons carry the thermal current towards the ablation surface. From figure 2 we see that, while the heater beams are on, the asymmetry is very large and blueshifted, indicative of heat flowing into the target. When the heater beams are off, the plasma cools and heat flows out of the target at a significantly reduced rate. Importantly, for a given heat flow different forms assumed for the electron distribution function predict different values of the asymmetry: thus the data shown in figure 2 provide information on the distribution function itself.

The form of the TS spectrum is determined by the dynamic form factor [23]:

$$S(\vec{k}, \omega) = \left| \frac{1 - G_i(\omega/k)}{1 - G_e(\omega/k) - G_i(\omega/k)} \right|^2 f_{0e}(\omega/k) + Z \left| \frac{G_e(\omega/k)}{1 - G_e(\omega/k) - G_i(\omega/k)} \right|^2 f_{0i}(\omega/k), \quad (3)$$

where  $G_s$  is the screening integral given by

$$G_s(\vec{v}_0) = \frac{4\pi Z_s^2 e^2}{m_s k^2} \int \frac{\vec{k} \cdot \vec{\nabla}_v f_{0s}(\vec{v})}{\vec{k} \cdot (\vec{v} - \vec{v}_0)} d\vec{v}, \quad (4)$$

where  $f_{0s}$  is the distribution function of the species ‘s’. At the ion acoustic resonance the real part of  $[1 - G_e - G_i]$  goes to zero, and the intensity of scattering will be determined by the complex part which, due to the pole in the integral, depends on the gradient of the distribution function in velocity space at the phase velocity of the wave.

For comparison with the experimental data we numerically solved the screening integrals to calculate TS spectra for two different distribution functions. The first is based on a simple SH model of the heat flow [24], whereas for the second distribution function we solved the FP problem (in the Lorentz approximation) in 1D using the FP code IMPACT [25]. The calculations took into account that the distribution function is probed at  $45^\circ$  to the plasma flow direction.

Figure 5 shows the comparison between the experimental data and the computed TS spectra for the FP and SH distribution functions where both carry the experimentally measured

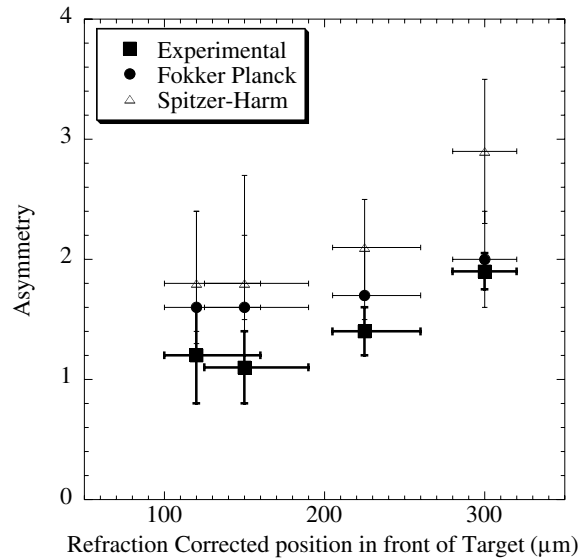


**Figure 6.** A comparison of the asymmetry from experiment (■), FP modelling (●) and SH modelling (△).

heatflow. For the 1D FP simulation, the density and temperature gradients ( $7 \text{ eV } \mu\text{m}^{-1}$ ) assumed were consistent with TS measurements at other positions in the plasma. However, in order to obtain a reasonable match between the experimental data and spectra predicted by the SH model at these densities and temperatures, the temperature gradient needed to be reduced to  $1.5 \text{ eV } \mu\text{m}^{-1}$ . Although, owing to the error bars in the data, this is not necessarily inconsistent with the measured temperature profile, the associated heat flow predicted by SH for such a temperature gradient— $Q = 4.2 \times 10^{13} \text{ W cm}^{-2}$ —is well below, and inconsistent with the experimentally measured values of the absorbed energy.

By quantifying an asymmetry we can use it to compare these two different thermal transport models. The ‘asymmetry’ is defined as the ratio of the integrated scattering under the blue and the redshifted peaks, divided at the Doppler-shifted probe wavelength. Figure 6 shows a plot of experimental and computed asymmetries at different points from the target surface. The error bars are larger closer to the target surface, owing to the effects of refraction. The errors in the computed asymmetries are associated with the uncertainties in the experimentally determined densities and temperatures. The FP model shows excellent agreement with experimental data, whereas SH thermal transport significantly over-estimates the asymmetry.

#### 4. Discussion

As shown above, if we associate a single temperature with the electrons then for the measured electron densities and temperatures we find a better fit to the Thomson spectra for the FP electron distribution than for the SH distribution. Specifically, the heat flow required for the SH simulations to fit the data is significantly less than that expected for these irradiances, thus providing support for the view that the FP distribution is more consistent with the data.

However, throughout the above analysis we have neglected the possible effects of resonance absorption. It is important to discuss this issue, as resonance absorption could

give rise to a hotter component to the electron distribution than the thermalized component, and thus our basic assumption of simply equating the outward enthalpy flux—calculated using a single electron temperature—with the heat flow at densities above the critical density is called into question.

Although there have been some previous measurements in the past of the degree of resonance absorption at these laser wavelengths and at these intensities, these data are difficult to apply to our particular circumstances. Although some measurements in spherical geometry, with the beams focused so as to illuminate a hemisphere, suggest that the fraction of the absorbed energy deposited as resonance absorption at the irradiance used in this experiment is up to 40% [26], other experiments, also in spherical geometry, but with much tighter focusing (such that the rays of each beam make a smaller angle of incidence to the target) suggest the fraction to be closer to 10%. Furthermore, code predictions for this irradiance (but again, in a geometry different to ours) predict resonance absorption of just over 11%.

It is important to note that the degree of resonance absorption is a function of the irradiation geometry. In our experiment the planar target was irradiated with a cone of beams, each with angle of incidence of  $10^\circ$ , and with mixed states of p- and s-polarization, and thus we do not immediately expect large amounts of resonance absorption. Strong resonance absorption typically depends on larger angles of incidence, increasing the electric field component of p-polarized light along the surface normal, coupled with ponderomotive self-steeping of the density gradient near critical [27] to reduce the evanescent propagation distance. Furthermore, random phase plates were used in our experiment (and not in the above cited work), and the local intensity fluctuations may also have an influence on the degree of resonance absorption.

Finally, the hallmark of resonance absorption (and indeed the method by which it has primarily been diagnosed in the past) is the observation of a multiple-temperature distribution in the bremsstrahlung emission from the plasma. In previous experiments, such multiple-temperature distributions have been diagnosed using information from filtered x-ray diodes. In the experiments described here we used a similar approach. The x-ray emission from the plasmas was imaged with x-ray pinhole cameras, and the radiation detected by a CCD. The x-ray intensity falling on the CCD over the majority of the image was such that there was, on average, less than one x-ray photon per pixel. In this single-photon mode, the energy of the incident photons can be measured from the number of counts recorded by an illuminated pixel [28]. An analysis of the number of photons incident upon the CCD as a function of photon energy is shown in figure 7. It can be seen that the data demonstrate a single temperature distribution, consistent with the experimentally measured temperatures. We expect the temperature inferred from this measurement to be less than the peak temperature measured at the critical surface, as the measurement is spatially averaged over the emitting region. However, and most importantly, the sensitivity of this measurement shows that a single temperature is consistent with the x-ray emission for over four orders of magnitude of x-ray intensity. This in turn allows us to make some conclusions about the fraction of hot electrons that could have been present. If we assume that the hot electron temperature for these conditions is of order 7 keV [29], then the fraction of the energy in this hot component must be less than 2% to be consistent with the CCD data. Such a small fraction would have a negligible effect on our analysis of the heat flow. Indeed, simulations of the Thomson scattered spectra indicate that the fraction of energy contained in such a hot-electron component would need to exceed 10% to significantly impact our analysis. In future one method that could be used to study the hot-electron component of the electron distribution function is measurements of the Thomson scattering electron feature. Whilst there would be no measurable change in the ion features until the number of hot electrons is on the order of the number of thermal electrons,

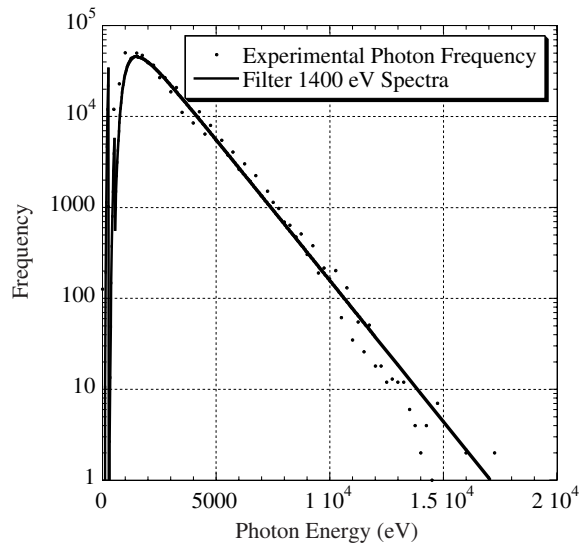


**Figure 7.** The frequency of x-ray photons recorded on the CCD as a function of photon energy. The solid line shows a fit to the data taking into account the response of the filter in front of the CCD, and assuming an average electron temperature over the emitting region of 1400 eV.

the addition of 0.01% hot electrons at 5 keV and 7 keV results in an increase in the scattered intensity of the electron features by 10 and 14 orders of magnitude, respectively.

## 5. Conclusion

In summary, we have used a  $4\omega$  probe to obtain Thomson scattering spectra at and above the critical density in a laser-produced plasma and have obtained a direct measurement of the heat flow. The asymmetry in the Thomson scattering spectra around the ion acoustic frequency gives information on the gradient of the distribution function at electron velocities corresponding to the phase velocity of the ion acoustic waves. The data agree well with Thomson scattering simulations based on a Fokker–Planck distribution function, but cannot be matched by simple Spitzer–Härm theory. As such this is the first direct confirmation of the Fokker–Planck models that have hitherto been shown to agree well with ablation pressures and rates.

## Acknowledgments

The authors would like to thank the staff of the Central Laser Facility at the Rutherford Appleton Laboratory. We are also very grateful to Professor Wojciech Rozmus from the University of Alberta and Professor Tony Bell from Imperial College, London, for useful discussions. R S Marjoribanks would like to acknowledge support from NSERC.

## References

- [1] Bobin J L 1971 *Phys. Fluids* **14** 2341
- [2] Delettrez J 1986 *Can. J. Phys.* **64** 932
- [3] Grey D R and Kilkenny J D 1980 *Plasma Phys.* **22** 81

- 
- [4] Yaakobi B and Bristow T C 1977 *Phys. Rev. Lett.* **38** 350
  - [5] Fabbro R, Fabre E, Amiranoff F, Garban-Labaune C, Virmont J, Weinfeld M and Max C E 1982 *Phys. Rev. A* **26** 2289
  - [6] Bell A R, Evans R G and Nicholas D J 1981 *Phys. Rev. Lett.* **46** 243
  - [7] Luciani J F, Mora P and Virmont J 1983 *Phys. Rev. Lett.* **51** 1664
  - [8] Albritton J R, Williams E A, Bernstein I B and Swartz K P 1986 *Phys. Rev. Lett.* **57** 1887
  - [9] Epperlein E M and Short R W 1991 *Phys. Fluids B* **3** 3092
  - [10] Alaterre P, Chenaispopovics C, Audebert P, Geindre J P and Gauthier J C 1985 *Phys. Rev. A* **32** 324
  - [11] Dahmani F and Kerdja T 1991 *Phys. Rev. A* **44** 2649
  - [12] Glenzer S H *et al* 1999 *Phys. Rev. Lett.* **82** 97
  - [13] Glenzer S H *et al* 1999 *Phys. Plasma* **6** 2117
  - [14] Chambers D *et al* 2002 *Phys. Rev. E* **66** 026410
  - [15] Chambers D *et al* 2001 *J. Quant. Spectrosc. Radiat. Transfer* **71** 237
  - [16] Chambers D 2003 private communications
  - [17] Amiranoff F, Fedosejevs R, Schmalz R F, Sigel R and Teng Y 1985 *Phys. Rev. A* **32** 3535
  - [18] Fabbro R, Max C and Fabre E 1985 *Phys. Fluids* **28** 1463
  - [19] Key M H, Toner W T, Goldsack T J, Kilkenny J D, Veats S A, Cunningham P F and Lewis C L S 1983 *Phys. Fluids* **26** 2011
  - [20] Chambers D 2001 *J. Quant. Spectrosc. Radiat. Transfer* **71** 383
  - [21] Cameron S M and Camacho J F 1995 *J. Fusion Energy* **14** 373
  - [22] Amiranoff F, Baton S D, Huller S, Malka V, Modena A, Mounaix P, Renard-LeGalloudec N, Rousseaux C and Salvati M 2000 *Phys. Rev. E* **61** 1949
  - [23] Evans D E and Katzenstein J 1969 *Rep. Prog. Phys.* **32** 207
  - [24] Spitzer L J and Härm R 1953 *Phys. Rev.* **89** 977
  - [25] Kingham R J and Bell A R 2004 *J. Comput. Phys.* **194** 1
  - [26] Keck R L, Goldman M C, Richardson W, Seka W and Tanaka K 1984 *Phys. Fluids* **27** 2762
  - [27] Fedosejevs R, Tomov I V, Burnett N H and Richardson M C 1977 *Phys. Rev. Lett.* **39** 932
  - [28] Janesick J, Elliott T, Marsh H H, Collins S, McCarthy J K and Blouke M M 1985 *Rev. Sci. Instrum.* **56** 796
  - [29] Estabrook K and Krueer W L 1978 *Phys. Rev. Lett.* **40** 42